Cement & Concrete Composites 33 (2011) 562–571

Contents lists available at ScienceDirect

Cement & Concrete Composites

journal homepage: www.elsevier.com/locate/cemconcomp

Modeling of the internal damage of saturated cement paste due to ice crystallization pressure during freezing

Lin Liu [a,b,*], Guang Ye [b,1], Erik Schlangen [b,2], Huisu Chen [a,3], Zhiwei Qian [b,4], Wei Sun [a,5], Klaas van Breugel [b,6]

[a] Jiangsu Key Laboratory of Construction Materials, School of Material Science and Engineering, Southeast University, Nanjing 211189, China
[b] Microlab, Faculty of Civil Engineering and Geosciences, Delft University of Technology, 2628CN Delft, The Netherlands

ARTICLE INFO

Article history:
Received 3 July 2010
Received in revised form 1 March 2011
Accepted 3 March 2011
Available online 9 March 2011

Keywords:
Frost action
Internal damage model
3D lattice fracture
Micro-cracks
Microstructure
Saturated cement paste

ABSTRACT

In order to quantify the internal damage of saturated cement paste caused by frost action, a damage model is proposed based on the thermodynamics of ice growth and fracturing of hydrated cement paste. According to the pore structure of cement paste from the HYMOSTRUC3D model, the penetration of crystals of ice through the pore network is simulated and stresses on the pore walls caused by the crystallization pressure of ice are first calculated. Then, the stresses in the solid skeleton of the microstructure of cement paste are calculated with the help of a three-dimensional (3D) lattice fracture model. Local damage, expressed as micro-cracks, is created if the local damage criterion is satisfied. The creation of micro-cracks in saturated cement paste during freezing is illustrated in this paper. The simulated results show that the number of micro-cracks in the microstructure of cement paste increases with decreasing temperature and the volume of cement paste increases with decreasing temperature when the temperature is below zero. To validate the model, strains of cement paste during freezing by simulations in this study are further compared with those by experiment. The reliability of the pore size distribution of cement paste by HYMOSTRUC3D simulation is also discussed.

1. Introduction

Deterioration of concrete caused by frost action (freezing and thawing cycles) is an important issue with regard to the service life of concrete structures in cold climates. The mechanism of frost damage has been investigated for several decades [1–5]. Powers indicated that harmful stresses could result from hydraulic pressure created by the volume increase when water transforms into ice [1]. Scherer argued that the primary source of stresses during freezing should be the crystallization pressure of ice, and not hydraulic pressure [3]. He gave evidence for the importance of crystallization pressure, for a case where hydraulic pressure would not be created, namely the experimental results from Beaudoin and MacInnis [5]. In their experiments, the length change of concrete during freezing was measured after the pore water had been exchanged with benzene. The fact is that the concrete still expanded, even through the volume of benzene decreases during freezing, and consequently no hydraulic pressure is created in this situation.

Based on the mechanism of frost damage, there are many competing theories to model cement-based materials exposed to freezing temperatures [4,6–8]. Nevertheless, only a few models provide a quantification of internal damage. Regarding the internal freezing damage of cement paste, there are still issues left unaddressed, such as how ice crystals form in the complex pore structure of cement paste, where and how the micro-cracks are created in the microstructure of cement paste, and how the microstructure of cement paste responds to the decreasing temperature. These questions are important for the analysis of freezing damage of cement-based materials, multi-scale modeling of concrete deterioration, and service life prediction. The aim of this study is to explore these issues.

In this paper, from a virtual microstructure of cement paste obtained from HYMOSTRUC3D [9–11], the ice growth process is captured as the temperature decreases. Stresses on the pore walls, locally exerted by crystals of ice, are calculated from the thermodynamics of ice growth and the geometric characteristics of the pores. The stresses in the solid skeleton of the microstructure can

* Corresponding author at: Jiangsu Key Laboratory of Construction Materials, School of Material Science and Engineering, Southeast University, Nanjing 211189, China. Tel.: +86 25 52090645; fax: +86 25 52090667.
E-mail addresses: LinLiuLinLiu@gmail.com (L. Liu), g.ye@tudelft.nl (G. Ye), H.E.J.G.Schlangen@tudelft.nl (E. Schlangen), chenhs@seu.edu.cn (H. Chen), Z.Qian@tudelft.nl (Z. Qian), sunwei@seu.edu.cn (W. Sun), k.vanbreugel@tudelft.nl (K. van Breugel).
[1] Tel.: +31 15 2784001; fax: +31 15 2786383.
[2] Tel.: +31 15 2786535; fax: +31 15 2786383.
[3] Tel.: +86 25 52090645; fax: +86 25 52090667.
[4] Tel.: +31 15 2789342; fax: +31 15 2786383.
[5] Tel.: +86 25 83795374; fax: +86 25 52090667.
[6] Tel.: +31 15 2784954; fax: +31 15 2786383.

0958-9465/$ - see front matter © 2011 Elsevier Ltd. All rights reserved.
doi:10.1016/j.cemconcomp.2011.03.001

be calculated with the help of a three-dimensional (3D) lattice fracture analysis [12,13]. Damage is created when the local damage criterion is satisfied. The creation of micro-cracks in the microstructure of cement paste is simulated and the volumetric dilation of saturated cement paste is obtained during the freezing process. Finally, the strain due to freezing and the simulated pore size distribution are discussed.

2. Theoretical background

During the freezing process, big flat crystals of ice are first formed when the temperature is below its freezing point, T_m. As the temperature subsequently decreases, the crystals of ice start to grow into small pores. The smaller the pore size, the lower the freezing point is, because of the surface contributions to the free energy. For a crystal of ice with a hemispherical end, at equilibrium, the relationship between its radius, r_c, and temperature, T, can be expressed as the well-known Gibbs–Thomson equation [3,4]:

$$r_c = -\frac{2\gamma_{cl}\cos\theta}{\Delta S_{fv}(T_m - T)} \quad (1)$$

where γ_{cl} is the energy of the water/ice interface, $\gamma_{cl} \approx 0.0409$ J/m^2 [3,4]. ΔS_{fv} is the entropy of fusion per unit volume of crystal. For ice, $\Delta S_{fv} \approx 1.2$ MPa/K [2–4]. θ is the contact angle between the crystal and the pore wall. In order to minimize the energy of the crystal, the contact angle is assumed as 180° and the crystal of ice is surrounded by a layer of liquid water [2]. Eq.(1) could then be rewritten as:

$$r_p = \frac{2\gamma_{cl}}{\Delta S_{fv}(T_m - T)} + \delta \quad (2)$$

where δ is the thickness of the liquid film between the crystal and the pore wall. In cement paste, $\delta \approx 1.0$–1.2 nm [14]. r_p represents the radius of a pore entry. It is the threshold for ice penetration into a pore. It indicates that the ice can grow into any saturated pores whose entrance is large enough according to Eq. (2).

If a small crystal of ice has the biggest curvature at its free end, κ^E_{cl}, its crystal pressure, p_c, can be given by Laplace's equation [2,15]:

$$p_c = p_l + \gamma_{cl}\kappa^E_{cl} \quad (3)$$

where p_l and p_c are the pressure in the liquid and the crystal. κ^E_{cl} is the curvature of the crystal/liquid interface at the free end of the crystal, m^{-1}. At the non-free sides of the crystal of ice, its curvature, κ^M_{cl}, may be smaller than that at the free end, κ^E_{cl}, due to the confinement of pore walls. Therefore an additional pressure, p_a, must be supplied by the pore wall to balance the crystal pressure, p_c. It could be expressed as [2,3,15]:

$$p_a = \gamma_{cl}\kappa^E_{cl} - \gamma_{cl}\kappa^M_{cl} = \gamma_{cl}\kappa^E_{cl}(1-\lambda) \quad (4)$$

where λ is a pore shape factor, which is in the range of 0–1. For a large pore with small entries, stresses on the pore walls are locally exerted by the crystals of ice because of the curvature difference. These stresses are assumed as the primary sources of stress which cause the frost damage of porous materials under the condition that the hydraulic pressure is negligible.

3. Modeling the freezing process of virtual cement paste

In this study, suppose that the nucleation of ice occurs at 0 °C, so that the ice grows slowly through the pores as the ambient temperature drops. In this case, the hydraulic pressure may be negligible. Therefore, the stresses on the pore walls are locally exerted by crystals of ice during the freezing process (see Eq. (4)). The stresses on the pore walls will result in stresses in the solid skeleton of the microstructure of cement paste. In order to calculate the stresses in the solid skeleton, a 3D lattice model is used. The 3D lattice structure is generated based on the connectivity of the hydrated cement particles. Local damage is caused if the local stress in the solid skeleton is high enough that the local damage criterion is satisfied. The flowchart of modeling the response of a microstructure of cement paste to the freezing process is shown in Fig. 1. The freezing process is divided into a series of temperature steps, ΔT_i. The initial input is a virtual 3D microstructure of cement paste and an initial temperature, T_0.

The computational procedure for determining the frost damage consists of the following steps: Step 1: the pore structure information is extracted from a virtual microstructure of cement paste and a corresponding 3D lattice structure based on the solids is also generated from the microstructure. Step 2: at the current temperature step, ΔT_k, crystals of ice, formed at any previous temperature step, penetrate into the pores whose entries satisfy Eq.(2). Step 3: the stresses on the pore walls are calculated according to Eq.(3). Step 4: the resultant forces on the pore walls are applied on the 3D lattice structure and the stress in the solid skeleton of the microstructure is calculated. Step 5: Determine if there is any local damage created according to the local damage criterion. If there is local damage created in the solid skeleton, the damage is considered as micro-cracks and a new microstructure of cement paste is formed. The computation then goes back to step 1. The newly formed microstructure is used as input for the next calculation until no additional local damage is created at the current temperature step. If no additional local damage is created, the temperature condition goes to the next temperature step, ΔT_{k+1}, and the computation goes to step 2. This is repeated until the freezing process is finished by reaching the final desired temperature.

3.1. Virtual microstructure of cement paste

The 3D microstructure of cement paste can be obtained from experiments or from numerical simulations. Experimental techniques, often used to detect the 3D microstructure of cement paste, include X-ray micro-tomography (micro-CT) [16], focused ion beam [17] and so on. The experimental results are influenced by limitations of resolution. Computer models, used to provide a microstructure of cement paste, include HYMOSTRUC3D [9–11], CEMHYD3D [18], μic [19] and so on. In this study, the microstructure of cement paste is simulated by the HYMOSTRUC3D model. Before hydration, 51,072 cement particles with a Blaine surface

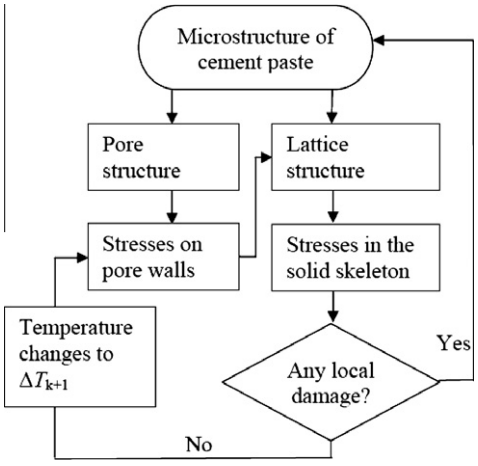

Fig. 1. Flowchart of modeling the response of a microstructure of cement paste on the freezing process.

area value of 420 m^2/kg and a discretized particle size distribution between 1 μm and 50 μm with an interval of 1 μm, are randomly distributed in a 3D body with the dimension of 100 × 100 × 100 μm^3. Periodic boundary conditions are utilized during the particle placement. CEM I 42.5 N with a potential Bogue phase composition of 64% C_3S, 13% C_2S, 8% C_3A, and 9% C_4AF by mass is used. The hydrating cement grains are simulated as growing spheres. As cement hydrates, the cement grains gradually dissolve and a porous shell of hydration products is formed around the grain. This results in an outward growth of particles. For cement paste with a water-to-cement ratio (w/c) of 0.4 at the degree of hydration (α) 0.69, a 3D image of the microstructure is shown in Fig. 2. In the 3D image of hydrated cement paste, the solid phases are, going from the center of a cement particle outwards, unhydrated cement particles (gray), inner hydration product (red) and outer hydration product (yellow), respectively. The corresponding pore structure of cement paste is shown in Fig. 3.

The pore size distribution of simulated cement paste can be obtained by dividing the 3D continuum microstructure into voxels of various sizes. The schematic diagram of computing the pore size distribution of a two-phase structure in 2D is illustrated in Fig. 4. For a voxel of size d_1, if it is totally occupied by pore phase, it is considered as a pore whose size is larger than d_1. If the voxel is partially occupied by solid phase and partially occupied by pore phase, it is considered to be a mixed-phase voxel. This voxel needs to be sub-divided further. After defining the new size of voxels as d_2, the phases comprising the newly formed voxels are determined. In this paper, d_2 is half of d_1. If one of the newly formed voxels is totally occupied by pore phase, it is assumed as a pore whose size is larger than d_2 but smaller than d_1. The simulated pore size distribution curve in 3D for cement paste with w/c = 0.4 at a degree of hydration of 0.69 is plotted in Fig. 5. The cumulative porosity with decreasing pore size and the differential curve are illustrated, respectively. In this case, the pore connectivity is not considered and it would seem to correspond best to the pore size distribution data obtained from an adsorption isotherm. However gas adsorption method is often used to characterize the pores up to 30 nm [20], which does not cover all the pore sizes in the simulation. A burning algorithm is utilized to determine the connectivity of pores of different sizes and a simulated MIP curve can be obtained

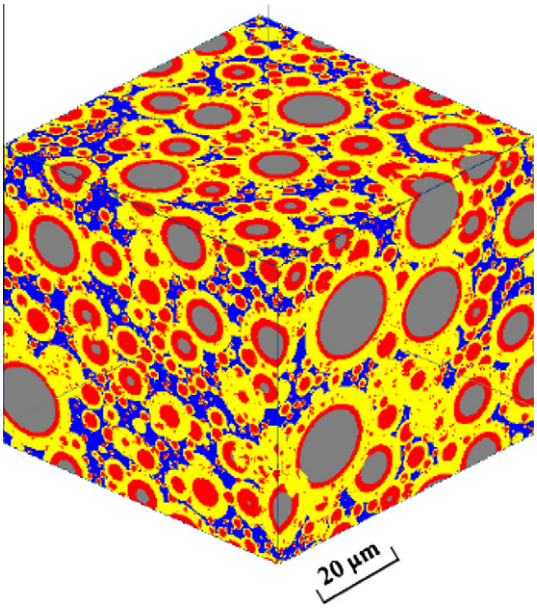

Fig. 2. 3D image of hydrated cement paste (w/c = 0.4, α = 0.69).

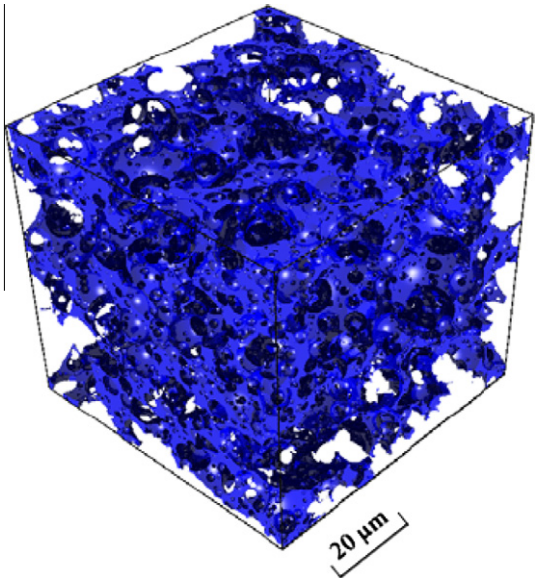

Fig. 3. Pore structure of hydrated cement paste (w/c = 0.4, α = 0.69).

[21].The pores' "burning" start from the surfaces of the 3D microstructure. The cumulative pore volume is the volume summation of all the connected pores at such a pore size. For example, the connected pores of size d_2 depend on the connectivity of pores with sizes no less than d_2. A discrepancy between the simulated pore structure and that obtained by mercury intrusion porosimetry (MIP) and SEM is found because of both computational and experimental limits. Those will be discussed in Section 5.1.

3.2. Pore structures during freezing

This section will show the progress as crystals of ice progressively penetrate through the pore network of cement paste. According to the IUPAC definition, there are three types of pores, i.e., micropores with diameters less than 2 nm, mesopores with diameters between 2 nm and 50 nm and macropores with diameters larger than 50 nm [20]. At the mesopore scale, the effects of in-pore confinement upon phase transition is dominant and the pore-size dependence of freezing point can be generally expressed as the Gibbs–Thomson equation (Eq. (1)) [4,22]. In this study, the freezing behavior of water in mesopores and macropores is dealt with. At the microscopic scale, local thermal equilibrium is assumed [23]. Therefore, at static equilibrium without temperature gradients, the freezing order of pores with different sizes as temperature decreases is given by Eq.(2). According to the condition for ice growing into smaller pores, when the temperature decreases to −1 °C, the crystal of ice can penetrate into any pore whose radius at the entrance is larger than 68 nm. When the temperature decreases to −20 °C, the condition for ice penetration is about r_p > 4.5 nm.

According the threshold of pore radius for ice growing in small pores (see Eq. (2)), the frozen and unfrozen pores are distinguished according to the following algorithm. For example, in a two-dimensional case, at a certain temperature T_1, a big crystal of ice is already formed, illustrated as "ice1" in Fig. 6. The other pores are filled with water. When the temperature decreases to T_2, the pore threshold that ice can grow into becomes r_p. The minimum distances of the pores between particles are calculated, i.e., the minimum distance of the pore between particles A and C is represented by l_{AC}, see Fig. 6. Since $l_{AC} > 2r_p$, the pore between particles A and C is filled with ice. Similarly, the ice can penetrate through the pore between particles A and D, because $l_{AD} > 2r_p$. However, the ice

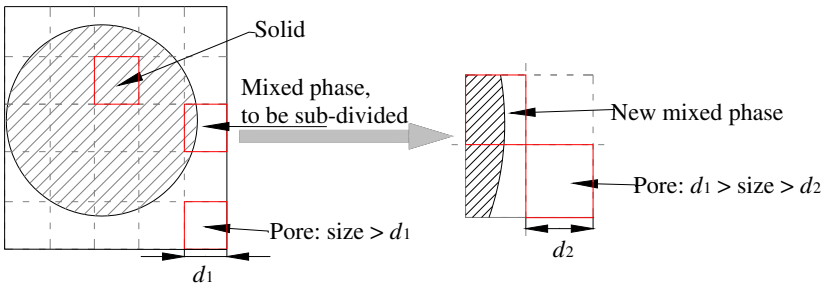

Fig. 4. 2D schematic diagram of computing the pore size distribution of a two-phase structure.

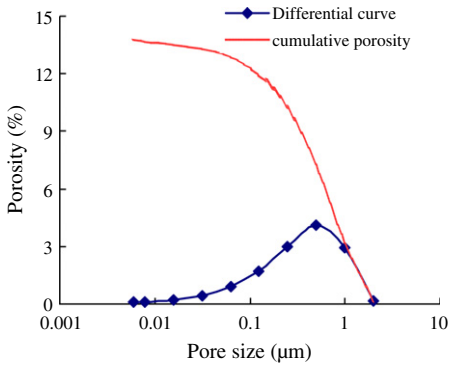

Fig. 5. Pore size distribution of hydrated cement paste (w/c = 0.4, α = 0.69).

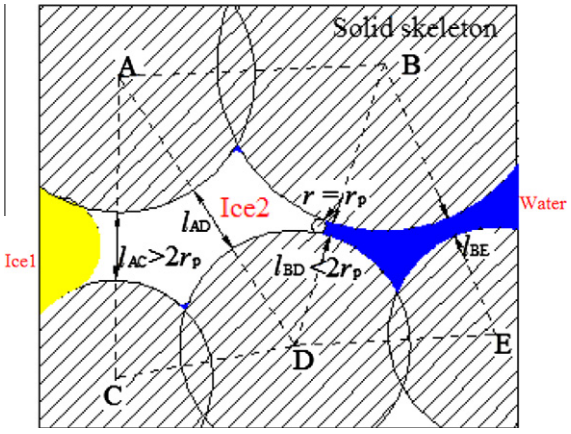

Fig. 6. 2D Schematic diagram of ice growth in irregular pores.

cannot penetrate through the pore between particles B and D, because $l_{BD} < 2r_p$. Then the pore space between these two particles is partially filled with ice and partially filled with water. The ice front goes to a circular arc, where a circle of a radius r_p is externally tangent to spheres B and D simultaneously. It means a crystal of ice with circular segment end r_p can be placed into the pore between particles A and D. The newly formed ice at temperature T_2 is illustrated as "ice2" (see Fig. 6). Since the ice cannot penetrate through the pore between particles B and D, the pore between particles B and E also remains unfrozen. In this way, all the pores between any two hydrated cement particles are judged to be frozen or unfrozen in the simulation. Fig. 6 illustrates the progressive growth of ice into smaller pores as the temperature decreases in the two-dimensional case. In this study, the modeling work is focusing on the situation in three dimensions. The algorithm for 3D is similar to that for 2D, except that the growing front of ice is a spherical cap, instead of a circular segment. At temperature T_2, the "ice1" can grow into any pore space where spherical caps with a radius r_p can infiltrate. The minimum distances of pores between any two hydrated cement particles can be calculated according to the positions and the diameters of particles, which are kept in computer memory.

At 0 °C, suppose the nucleation of ice starts from the surfaces of the microstructure. Then, the crystals of ice penetrate through the pore network from the outside in. An example of the pore space of cement paste during freezing is shown in Fig. 7. At $T = -0.2$ °C, the unfrozen space of pores where water remains unfrozen is illustrated in Fig. 7a, and the frozen space of pores where water turns into ice is illustrated in Fig. 7b. The ice saturation, Φ_C, (i.e., the ratio of the ice volume to the total volume of capillary pores) is temperature-dependent. For cement paste with w/c = 0.4 at the degree of hydration 0.69, the curve of Φ_C versus temperature is plotted in Fig. 8. The curve shown in Fig. 8 is different from the data in the literature [4]. This might because the pore structure from HYMOSTRUC3D might provide more open networks relative to a real cement paste for ice penetration. The percolation threshold of capillary porosity is about 3.5% in the HYMOSTRUC3D model, while is about 20–22% in the NIST model [26]. The simulated ice saturation curve during freezing does not correspond well to the experimental results in [4,24,25]. Due to super cooling effects, the ice nucleation may not happen at 0 °C.

In concrete science, mesopores cover a large amount of capillary pores and gel pores. Attention should be drawn to the fact that the size division of capillary and gel porosity is to a large extent arbitrary and there is no agreement between different researchers [20,27,28]. Experimental studies on cement pastes indicate that the freezing of water in C–S–H gel pores takes place at least below −23 °C [24,25,29]. Therefore, it is reasonable to consider that the freezing of gel pores does not take place in the temperature range of 0 °C to −20 °C. Assuming gel pores are smaller than 8 nm (the frozen threshold at −23 °C according to Eq. (2)), the pore space mentioned in this paper refers to the capillary pores. Based on the virtual microstructure of cement paste from HYMOSTRUC3D, the gel pores are included in the C–S–H product and are considered as an intrinsic part of the C–S–H gel.

3.3. Stresses on pore walls

The foregoing indicates that the developed pressure for the crystal of ice is dependent on the curvature difference between the crystal/liquid interface and the pore walls (see Eq. (4)). For simplicity for explaining the frost damage [2,8], the shape of the pores is often assumed as cylindrical or spheroidal. For a cylindrical pore with a radius of r_p, see Fig. 9a, at the hemispherical end of the crystal, the curvature is $\kappa_{cl}^{E} = 2/(r_p - \delta)$. At the cylindrical sides of the crystal, the curvature is $\kappa_{cl}^{M} = 1/(r_p - \delta)$. It follows that the imposed pressure by the pore wall is $p_a = \gamma_{cl}/(r_p - \delta)$. In this case, the pore shape factor λ equals 0.5.

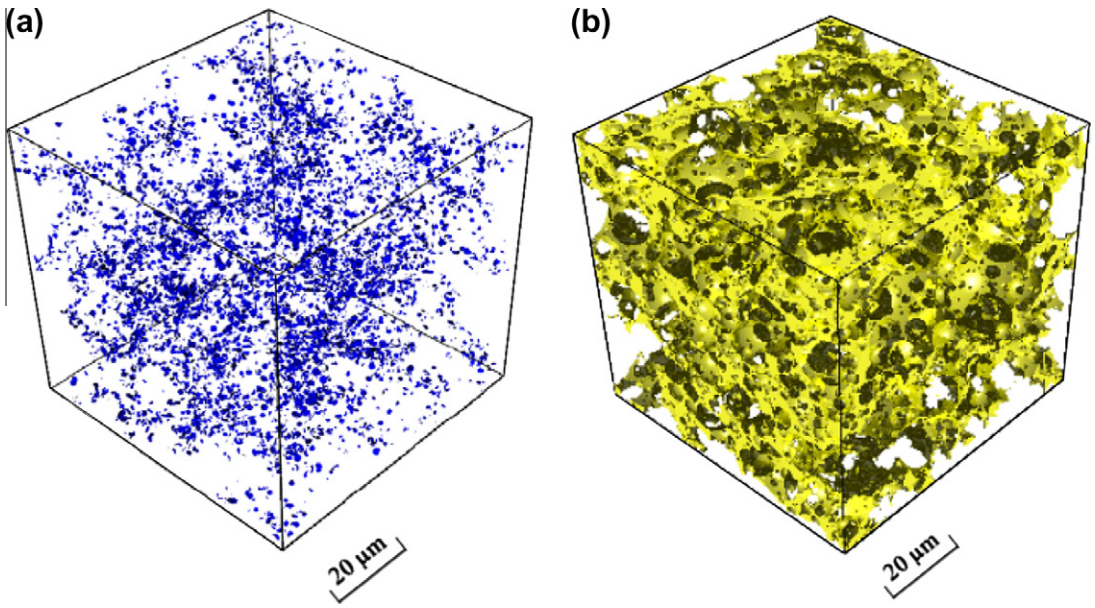

Fig. 7. At $T = -0.2$ °C, (a) Pore space where water remains unfrozen. (b) Pore space where water turns into ice (cement paste with $w/c = 0.4$, $\alpha = 0.69$).

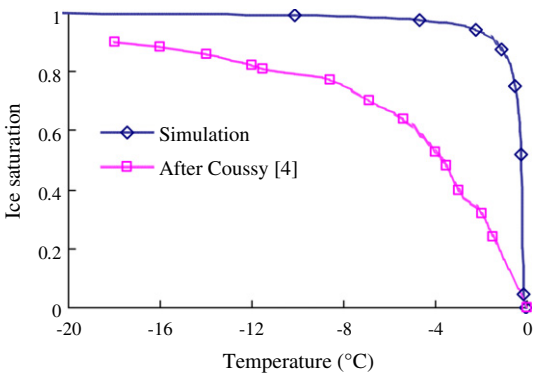

Fig. 8. Ice saturation (Φ_C) of cement paste ($w/c = 0.4$) versus temperature from simulation ($\alpha = 0.69$) and from literature [4] (hydration 28 days) on freezing process.

However, the shape of pores in cement paste is not regular because of its complex microstructure. In this situation, the crystals of ice still grow into pores which satisfy the condition for ice penetration. Fig. 9b shows the growth of ice in the irregular pores of hardened cement paste. At the free end of the ice, its shape is still assumed to be hemispherical and the curvature is, $\kappa_{cl}^{E} = 2/(r_p - \delta)$. At the confined side of the ice, however, its curvature is dependent on the curvature of the irregular pore walls. Hydrated cement particles constitute the solid skeleton of cement paste, which are acting in the role of pore walls. If the radius of a hydrated cement particle is R_{hc} (see Fig. 9b), then it is curvature is $2/(R_{hc} + \delta)$. For ice at the confined side which is in contact with this hydrated cement particle, its curvature then is, $\kappa_{cl}^{M} = -2/(R_{hc} + \delta)$. It follows that the imposed pressure by the pore wall is $p_a = 2\gamma_{cl}/(r_p - \delta) + 2\gamma_{cl}/(R_{hc} + \delta)$. Because $R_{hc} \gg r_p$, $p_a \approx 2\gamma_{cl}/(r_p - \delta)$. The pore shape factor λ approaches 0. According to the principle of mechanical equilibrium, stresses on the pore walls, $\boldsymbol{\sigma_c}$, are exerted by the crystals of ice simultaneously. The stress on the pore wall, $\boldsymbol{\sigma_c}$, is equal to $\boldsymbol{p_a}$ but with an opposite direction. The stresses on the pore walls will result in stresses in the solid skeleton of cement paste, and consequently can cause local damage in the cement paste. The following procedure is developed to capture the damage

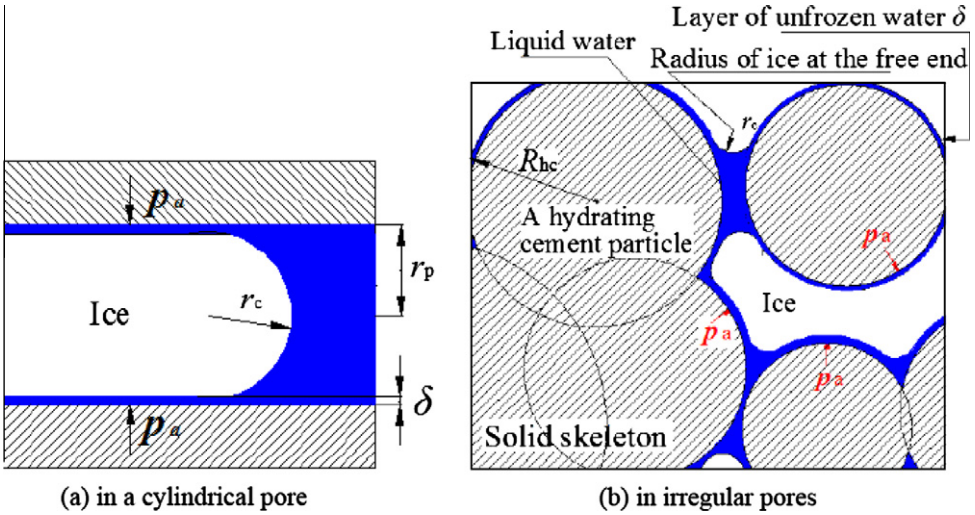

Fig. 9. Crystallization of ice in small pores.

locally created in the microstructure of cement paste during the freezing process.

3.4. Resultant forces caused by frost action

The resultant force on each hydrated cement particle is an integration of the stress generated on the pore wall $\boldsymbol{\sigma_c}$ on the surfaces $\boldsymbol{\partial\Omega_c}$. $\boldsymbol{\partial\Omega_c}$ represents the surfaces of the hydrated cement particle that is in contact with ice. It can be written as:

$$\mathbf{f}_i = \int_{\partial\Omega_c} \boldsymbol{\sigma_c} \cdot \boldsymbol{\partial\Omega} \tag{5}$$

where $\mathbf{f}_i$ is a tensor, representing the external force on the ith hydrated cement particle. $\boldsymbol{\sigma_c}$ represents the stress generated on the pore wall and can be obtained according to Section 3.3. As shown in Fig. 10, for the hydrated cement particle A, the surfaces that are in contact with ice, are represented by $\boldsymbol{\partial\Omega_{c1}}$ and $\boldsymbol{\partial\Omega_{c2}}$, respectively. The stresses on the surface $\boldsymbol{\partial\Omega_{c1}}$ and $\boldsymbol{\partial\Omega_{c2}}$ are $\boldsymbol{\sigma_{c1}}$ and $\boldsymbol{\sigma_{c2}}$, respectively. The resultant force on hydrated cement particle A, $\mathbf{f}_A$, is:

$$\mathbf{f}_A = \int_{\partial\Omega_{c1}} \boldsymbol{\sigma_{c1}} \cdot \boldsymbol{\partial\Omega} + \int_{\partial\Omega_{c2}} \boldsymbol{\sigma_{c2}} \cdot \boldsymbol{\partial\Omega} \tag{6}$$

Then the resultant force, $\mathbf{f}_A$, is imposed at the center of particle A, see Fig. 10. Similarly, the resultant force on hydrated cement particle B, $\mathbf{f}_B$, can be calculated and imposed at the center of particle B. In this way, all the resultant forces on each hydrated cement particle can be established in the 3D microstructure of the hydrated cement paste.

3.5. Fracturing of the lattice structure of cement paste

To obtain the stress in the solid skeleton of the microstructure, a 3D lattice structure of cement paste is first generated according to the following principles:

Every hydrated cement particle is considered as a node and every two connected hydrated cement particles are considered as one beam element. The geometry parameter of a beam element (l and h) is determined by the distance between the two nodes and the diameter of the contact area with which two hydrated cement particles are connected (see Fig. 11). The Young's modulus and shear modulus (E_n, G_n) of a node are the weighted averages of those of its component solid phases, and the Young's modulus and shear modulus (E, G) of an element are the weighted averages of those of its two component nodes [13,30]. A lattice structure of cement paste with w/c = 0.4 at 0.69 degree of hydration is shown in Fig. 12.

The next step is to define the boundary conditions for the lattice structure and to apply the forces caused by ice crystallization on each node. Here, free expansion of the sample is assumed. The forces caused by ice crystallization are obtained and imposed on each node according to Section 3.4 and then a stress analysis is conducted. The stress analysis, in principle, is a sequence of elastic stress calculations for the lattice structure. A detailed description of the lattice analyses of cement paste can be found in the literature [31]. It is assumed that when the tensile stress is larger than the tensile strength of a beam element, the beam element fractures. This is the local damage criterion. The tensile strength of an element is determined based on its weakest zone by weighted averaging. As shown in Fig. 11, the weakest zone is on plane AB, and the tensile strength of the element, f_t, is:

$$f_t = \frac{R_i^2}{R_o^2} f_i + \frac{R_o^2 - R_i^2}{R_o^2} f_o \tag{7}$$

where R_i and R_o represent the radii of inner product and outer product for the cross-section, respectively. f_i and f_o represents the tensile strength of inner product and outer product, respectively. The values of elastic properties and tensile strength of solid phases are listed in Table 1 [32–34]. Research is ongoing to determine the true relationship between tensile stress analyzed with the model and tensile strength of the local material. This might lead to corrections in a later stage, because of model parameters and size effects on strength.

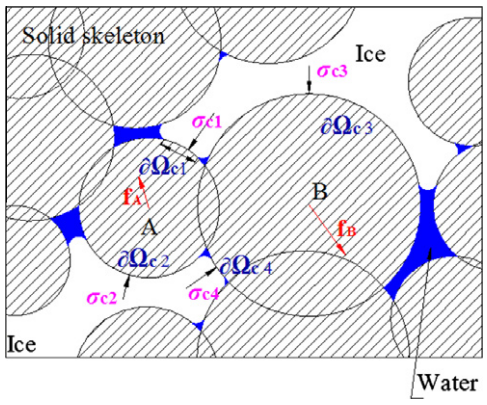

Fig. 10. 2D Schematic diagram of imposing resultant forces in the microstructure of cement paste.

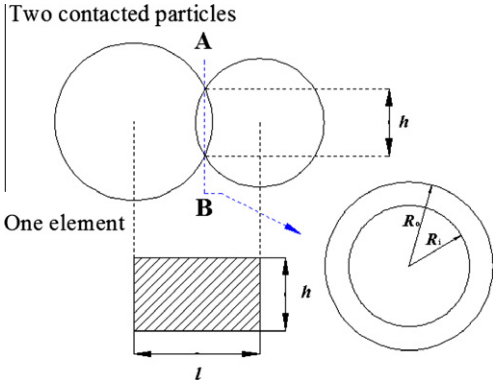

Fig. 11. Schematic of generation of one beam element [13,30].

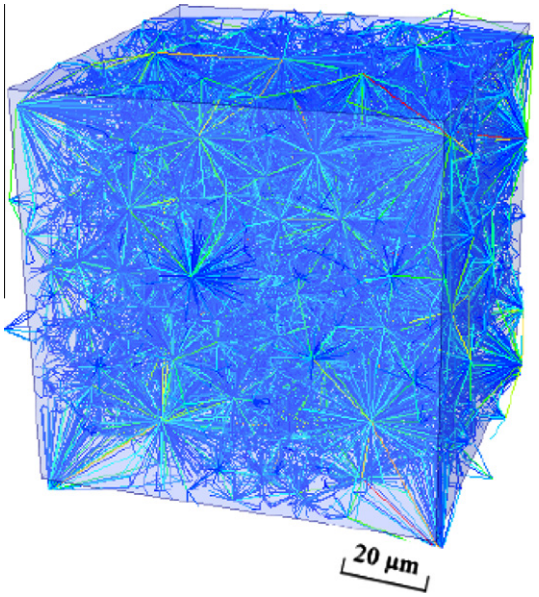

Fig. 12. 3D lattice mesh of hydrated cement paste (w/c = 0.4, α = 0.69).

Table 1
Elastic properties and tensile strength of solid phases [32–34].

Solid phase	Young's modulus E (GPa)	Shear modulus G (GPa)	Tensile strength (GPa)
Unhydrated cement	135	52.0	1.80
Inner product	30	12.0	0.24
Outer product	22	8.9	0.15

In the stress analysis of the 3D lattice model, the displacement of each node (i.e. hydrated cement particle) can be obtained. Therefore, the new position of every hydrated cement particle is known. Then the volume change of the 3D microstructure of cement paste can be calculated. At every temperature step, by calculating the cube length of the structure, the volume change of cement paste can be predicted. In this study, the solid shrinkage is taken into account as the temperature decreases. The thermal expansion of the solid skeleton, in terms of length change of a beam element, is calculated according to the following equation:

$$\Delta l = \alpha_s \cdot (T - T_0) \cdot l \tag{8}$$

where Δl is the length change of the beam element because of a temperature change. l is the initial length of the beam element. α_s is the linear thermal dilation coefficient of the solid skeleton. α_s is generally adopted as the thermal coefficient of mortar or concrete without phase transformation in pores, $\alpha_s = 10 \times 10^{-6}\,K^{-1}$ [3,15]. T is the current temperature and T_0 is the initial temperature. After calculating the length change of every beam element, the final displacements of nodes can be obtained. The final displacement of a node is a summation of the displacement caused by the thermal effect and that caused by ice crystallization. Since a boundary condition of free expansion is used, the stress in the solid skeleton contributed by the thermal effect is zero. The thermal expansion of ice during freezing is ignored, even if the thermal expansion coefficient of ice ($50 \times 10^{-6}\,K^{-1}$ [3,15]) is higher than that of the solid skeleton. Because as temperature drops, ice contracts more than the solid skeleton, and the gaps between the crystals of ice and solid pore walls will be compensated by being filled with water/ice through water flow. One of the basic assumptions in this study is that the nucleation occurs at 0 °C and ice is formed in static equilibrium. Therefore, excess water can be driven out and nearly no hydraulic pressure is generated in the microstructure. In this case, the stresses on walls will be exerted by ice only because of the curvature difference according to Eq. (4). And the thermal expansion effect of ice does not contribute to the harmful stresses during the freezing process. Conversely, the thermal expansion of ice will contribute to the damage of the microstructure during the heating process, because it expanses more than the solid skeleton.

3.6. The role of micro-cracks

The fracturing of beam elements results in the creation of micro-cracks in the microstructure of cement paste. The micro-cracks are assumed to have the shape of a cylinder. For the newly created micro-crack, its length L_c is the elongation of the element (see Fig. 13a and b) and its cross-section is equal to the cross-section of the element. The micro-crack behaves as a pore, which is assumed to be filled with water or ice during freezing. When the size of the micro-crack is small, $L_c < 2r_p$, the micro-crack is assumed to be filled with water (see Fig. 13c). When $L_c \geqslant 2r_p$, the crystal of ice can penetrate into it. The freezing of water in micro-cracks will contribute to stresses in the solid skeleton, as illustrated in Fig. 13d. This may cause severe damage.

According to the flowchart of the simulation (see Fig. 1), the freezing process is sub-divided into a series of temperature steps.

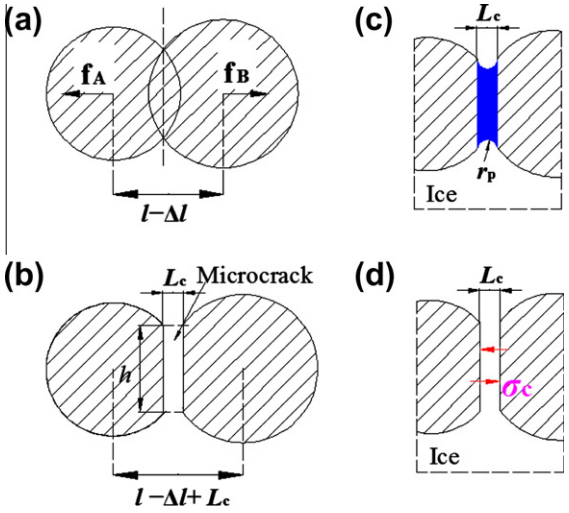

Fig. 13. Schematic representation of a micro-crack created due to freezing.

At a certain temperature, micro-cracks are created. When temperature further decreases, new micro-cracks are created. To distinguish the micro-cracks created at different temperatures, they are divided into old micro-cracks and new micro-cracks. The old micro-cracks are created before the current temperature step and the new micro-cracks are created at the current temperature step. It should be noted that the length of the old micro-cracks will change at different temperatures steps, because the position of the nodes will change as the temperature decreases.

4. Simulation results

The damage introduced by ice crystallization could be represented by broken elements in the lattice structure. Fig. 14 shows the creation of micro-cracks (i.e., broken elements) in a 3D lattice structure of hydrated cement paste ($w/c = 0.4$, $\alpha = 0.69$) at progressively decreasing temperatures. The interval of the temperature steps is 1 °C. It is found that the micro-cracks are created randomly. The weak beam elements which are subjected to tensile stress break first. As the temperature decreases, relatively stronger beam elements break. It also can be observed that the number of micro-cracks increases with the decreasing temperature.

The number of micro-cracks can be quantitatively predicted with the decreasing temperature. The number of micro-cracks versus temperature is illustrated in Fig. 15. It indicates that the degree of damage of cement paste contributed by ice crystallization increases with decreasing temperature. Because the lower the temperature is, the higher is the pressure applied on pore walls according to Eq.(2) and Eq.(4). Although Fig. 8 shows nearly all of the ice was formed at −1 °C, the pressure applied on the pore walls by ice at −1 °C is not large enough to break a lot of elements.

The volumetric dilation of cement paste obtained from the simulation is shown in Fig. 16. As the temperature decreases, the volumetric change of saturated cement paste is caused by thermal expansion and crystallization pressure of ice. When the temperature is above 0 °C, the volume change of the microstructure is only caused by the thermal expansion/shrinkage of the solid skeleton. The cement paste shrinks uniformly due to the decreasing temperature. When the temperature is below 0 °C, cement paste expands upon freezing. The contribution to volume change from the crystallization pressure of ice is more than that from thermal expansion. A comparison of strains by simulation and by experiments is discussed in Section 5.2.

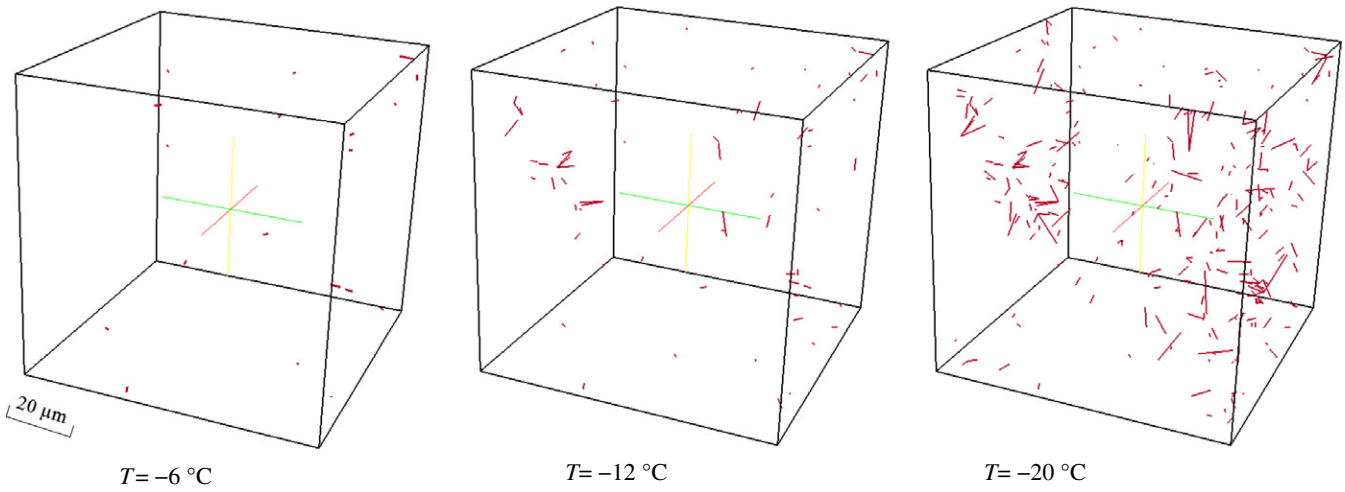

Fig. 14. Micro-cracks created in cement paste at different temperatures (w/c = 0.4, α = 0.69).

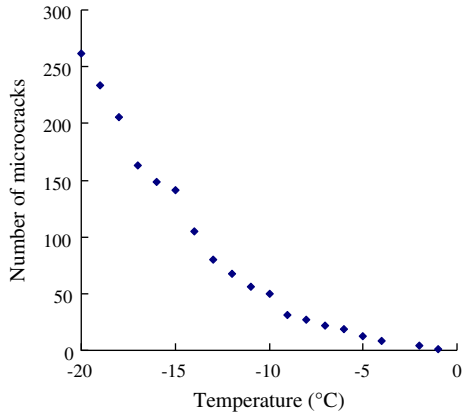

Fig. 15. The number of micro-cracks in the microstructure of cement paste with decreasing temperature (w/c = 0.4, α = 0.69, cube length = 100 μm).

5. Discussion

5.1. Comparison of pore size distributions by simulation and by experimental techniques

As indicated in Section 3.2, the pore structure of cement paste is important for analyzing the freezing behavior of cement paste. Therefore the reliability of the simulated pore structures (i.e., pore size distribution) of cement paste by HYMOSTRUC3D simulation is discussed in the current study. By use of a burning algorithm on the 3D microstructure, a MIP pore size distribution is simulated. The pore size distribution by simulation is compared with those measured by standard MIP test [11], pressurization-depressurization cycling (PDC) MIP test [35] and BSE images analysis [11], see Fig. 17. The specimens used by those experiments are ordinary Portland cement pastes (CEMI 42.5 N, w/c 0.4) with 28 days hydration. According to the cement hydration model HYMOSTRUC3D, the degree of hydration of cement paste (CEMI 42.5 N, w/c = 0.4) is about 0.69 after hydration for 28 days.

By comparing to experiments, it is observed that the shape of the simulated pore size distribution curve is similar to those obtained by processing BSE images of cement paste and the PDC-MIP test. "An 'accessible effect'" can be obviously observed when the pore size is no less than 1 μm and disappears at 0.5 μm in the simulation, because pore percolation occurs at 0.5 μm pore size. Discrepancies of the pore size distribution between simulation and experimental tests shown in Fig. 17 might result from some basic assumptions in cement paste simulation from the HYMOSTRUC3D model. The pores with sizes larger than 2 μm are not seen in the simulation, while they exist in the experimental results. This may be related to the real world flocculation of cement particles, which is not included in the HYMOSTRUC3D simulation. Because of computational limitations, the minimum diameter of

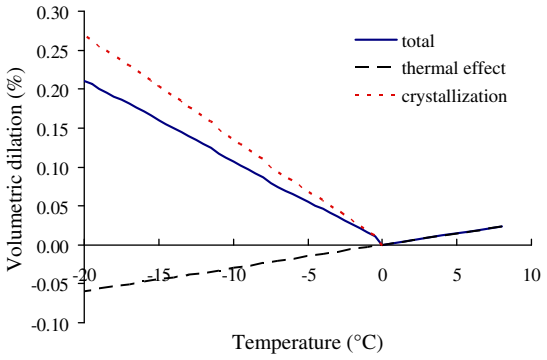

Fig. 16. Contributions to the volumetric dilation of cement paste (w/c = 0.4, α = 0.69) with decreasing temperature.

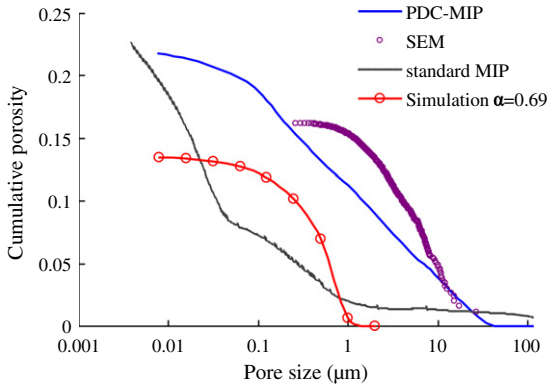

Fig. 17. Pore size distributions of cement paste by HYMOSTRUC3D simulation, standard MIP test [11], PDC-MIP test [35] and BSE image analysis [11] (CEMI 42.5 N, w/c 0.4, age 28 days).

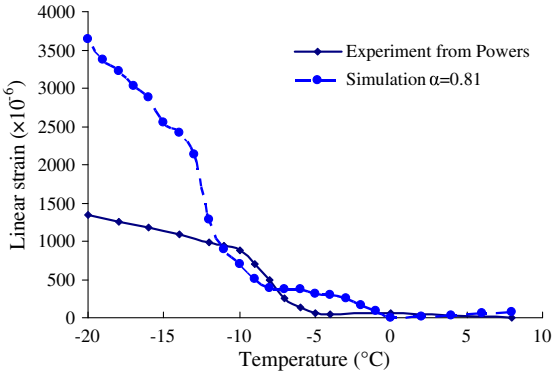

Fig. 18. Linear strains of saturated cement paste during freezing obtained by simulation and by experiments (after Powers [36]).

cement particles is assumed to be 1 μm in this study. However, real cements have a certain number of particles with sizes smaller than 1 μm. Additionally, HYMOSTRUC3D models hydration as the expansion of concentric shells around the original cement particles and does not include precipitation of products such as calcium hydroxide within the pore spaces between particles. A detailed discussion about the pore structure characteristics with the HYMOSTRUC3D model can be found in literature [26].

5.2. Comparison of strains by simulations and by experiments

The simulated linear strain of cement paste during freezing is compared with the experimental result from Powers [36], see Fig. 18. For cement paste with *w/c* of 0.6, the discrepancy between the measured and simulated strains is significant. A delayed nucleation is observed from the experiment. Crystals of ice nucleate at a temperature of about −5 °C. This might be the reason that, in the temperature range of −1 °C to −7 °C, the experimental result is lower than the simulated one, which assumes that nucleation occurs at 0 °C. The simulated strain is higher than that by experiments when the temperature is lower than −12 °C. This might result from the experimental conditions. Experimental results may be influenced by the temperature decreasing rate, the specimen size, the saturation degree of specimens and so on. In addition, the microstructure of cement paste from HYMOSTRUC3D model has a high connectivity of capillary pores [26]. As a consequence, the ice propagation through the pore network might be faster than that in real cement paste specimens (see Fig. 8).

6. Conclusion

Based on the assumption that the primary source of stress during freezing is the crystallization pressure of ice, the internal damage of saturated cement paste exposed to low temperatures is simulated at a microscopic scale. On the basis of a virtual microstructure of cement paste obtained from HYMOSTRUC3D, the formation of ice in the pore structure of cement paste is simulated. The microstructural change of cement paste is analyzed and the creation of micro-cracks in the microstructure of saturated cement paste is predicted quantitatively. The simulated results show that the number of micro-cracks increases with the decreasing temperature and the volumetric dilation of cement paste increases with decreasing temperature when the temperature is below zero. By comparing to experimental results, it is found that the overall high connectivity of the HYMOSTRUC3D pore structure with its stated percolation threshold of 3.5% is considered as a major contribution to the differences between experimental and model results in Figs. 8, 17 and 18.

This study focused on assessing the internal damage of cement paste caused by the crystallization pressure of ice during the freezing process. The influence of liquid pressure is not considered under a drained condition at the microscopic scale. The assessment of the internal damage caused by hydraulic pressure and a comparison with the internal damage caused by ice crystallization will be studied in future research. In addition to the internal damage of saturated cement paste, this model will be extended to consider the effects of air voids and the cryo-suction action during the freezing process in the future.

The damaged microstructure of cement paste provides information for predicting mechanical and transport properties of cement paste through its life and can be used as an input for multi-scale modeling of concrete or mortar properties. A future study will be devoted to a systematic comparison of the numerical results with experimental data.

Acknowledgements

The financial support of the National Basic Research Program (973 Program) of China via Grant No. 2009CB623203 and National Natural Science Foundation of China via Grant No. 50708018, is greatly acknowledged. The financial support of China Scholarship Council is also greatly acknowledged.

References

[1] Powers TC. The air requirement of frost-resistant concrete. Proc Highway Res Board 1949;29:184–211.
[2] Scherer GW. Crystallization in pores. Cem Concr Res 1999;29(8):1347–58.
[3] Scherer GW, Valenza JJ. In: Young F, Skalny J, editors. Mechanisms of frost damage, materials science of concrete VII. American Ceramic Society; 2005.
[4] Coussy O, Monteiro P. Poroelastic model for concrete exposed to freezing temperatures. Cem Concr Res 2008;38(1):40–8.
[5] Beaudoin JJ, MacInnis C. The mechanism of frost damage in hardened cement paste. Cem Concr Res 1974;4(2):139–47.
[6] Bazant ZP, Chern J-C. Mathematical model for freeze-thaw durability of concrete. J Am Ceram Soc 1988;71(9):776–83.
[7] Hain M, Wriggers P. Computational homogenization of micro-structural damage due to frost in hardened cement paste. Finite Elem Anal Des 2008;44(5):233–44.
[8] Zuber B, Marchand J. Modeling the deterioration of hydrated cement systems exposed to frost action Part I: description of the mathematical model. Cem Concr Res 2000;30(12):1929–39.
[9] van Breugel K. Simulation of hydration and formation of structure in hardening cement-based materials. PhD thesis, Delft University of Technology, Delft; 1991. <http://Microlab.citg.tudelft.nl>.
[10] Koenders E. Simulation of volume changes in hardening cement-based materials. PhD thesis, Delft University of Technology, Delft; 1997. <http://Microlab.citg.tudelft.nl>.
[11] Ye G. Experimental study and numerical simulation of the development of the microstructure and permeability of cementitious materials. PhD thesis, Delft University of Technology, Delft; 2003. <http://Microlab.citg.tudelft.nl>.
[12] Schlangen E. Experimental and numerical analysis of fracture processes in concrete. PhD thesis, Delft University of Technology, Delft; 1993. <http://Microlab.citg.tudelft.nl>.
[13] Qian Z. 3D lattice analysis of cement paste. Master thesis, Delft University of Technology, Delft; 2008.
[14] Sun Z, Scherer GW. Pore size and shape in mortar by thermoporometry. Cem Concr Res 2010;40(5):740–51.
[15] Sun Z, Scherer GW. Effect of air voids on salt scaling and internal freezing. Cem Concr Res 2010;40(2):260–70.
[16] Promentilla MAB, Sugiyama T, Hitomi T, Takeda N. Quantification of tortuosity in hardened cement pastes using synchrotron-based X-ray computed microtomography. Cem Concr Res 2009;39(6):548–57.
[17] Trtik P, Münch B, Lura P. A critical examination of statistical nanoindentation on model materials and hardened cement pastes based on virtual experiments. Cem Concr Compos 2009;31(10):705–14.
[18] Bentz DP, Garboczi EJ. Percolation of phases in a three-dimensional cement paste microstructure model. Cem Concr Res 1991;21(2–3):325–44.
[19] Bishnoi S, Schrivener KL. μic: a new platform for modeling the hydration of cements. Cem Concr Res 2009;39(4):266–74.
[20] Aligizaki KK. Pore structure of cement-based materials: testing, interpretation and requirements. Taylor and Francis; 2006.
[21] Stauffer D. Introduction to percolation theory. London: Taylor and Francis; 1985.

[22] Morishige K, Kawano K. Freezing and melting of water in a single cylindrical pore: the pore-size dependence of freezing and melting behavior. J Chem Phys 1999;110(10):4867–72.
[23] Setzer MJ. Frost suction as the basic mechanism of frost action. In: Kovler K, editor. International RILEM-JCI seminar on concrete durability and service life planning ConcreteLife'06, Dead Sea, Israel; 2006. p. 155–66.
[24] Bentz DP. Low temperature calorimetry studies of hydrating portland cement pastes. NISTIR 7267, US Department of Commerce; October 2005. <http://www.fire.nist.gov/bfrlpubs/build05/art051.html>.
[25] Bentz DP. Lithium, potassium, and sodium additions to cement pastes. J Adv Cem Res 2006;18(2):65–70.
[26] Ye G, van Breugel K, Fraaij ALA. Three-dimensional microstructure analysis of numerically simulated cementitious materials. Cem Concr Res 2003;33(2):215–22.
[27] Mindess S, Young JF. Concrete. Englewood Cliffs (NJ): Prentice-Halls; 1981.
[28] Metha PK, Monteiro PJM. Concrete: microstructure, properties and materials. McGraw-Hill; 2006.
[29] Setzer MJ. Micro-ice-lens formation in porous solid. J Colloid Interf Sci 2001;243(1):193–201.
[30] Tan L. Failure mechanisms in hydrating cement particle systems. Master thesis, Delft University of Technology, Delft; 2007.
[31] Qian Z, Schlangen E, Ye G, van Breugel K. Prediction of mechanical properties of cement paste at microscale. Mater Constr 2010;60(297):1–12.
[32] Manzano H, Dolado JS, Ayuela A. Elastic properties of the main species present in Portland cement pastes. Acta Mater 2009;57(5):1666–74.
[33] Qian Z, Ye G, Schlangen E, van Breugel K. 3D lattice fracture model: application to cement paste at microscale. Key Eng Mater 2011;452–453:65–8.
[34] Sanahuja J, Dormieux L, Chanvillard G. Modeling elasticity of a hydrating cement paste. Cem Concr Res 2007;37(1):1427–39.
[35] Zhou J, Ye G, van Breugel K. Characterization of pore structure in cement-based materials using pressurization–depressurization cycling mercury intrusion porosimetry (PDC-MIP). Cem Concr Res 2010;40(7):1120–8.
[36] Powers TC. The physical structure and engineering properties of concrete. Res Develop Lab Portland Cem Assoc Bull 1958;90:1–28.